Available online at www.sciencedirect.com
ScienceDirect
Journal of Nuclear Materials 373 (2008) 123–129
journal of nuclear materials
www.elsevier.com/locate/jnucmat

# Structural evolution of zirconium carbide under ion irradiation

D. Gosset [a,*], M. Dollé [b], D. Simeone [a], G. Baldinozzi [c], L. Thomé [d]

[a] CEA Saclay, DEN/DMN/SRMA, F-91191 Gif/Yvette cedex, France
[b] CEMES-CNRS (UPR 8011), BP 94347, F-31055 Toulouse cedex 4, France
[c] SPMS, Ecole Centrale Paris, F-92295 Châtenay-Malabry cedex, France
[d] CSNSM, bat. 108, F-91405 Orsay, France

Received 1 April 2007; accepted 16 May 2007

**Abstract**

Zirconium carbide is one of the candidate materials to be used for some fuel components of the high temperature nuclear reactors planned in the frame of the Gen-IV project. Few data exist regarding its behaviour under irradiation. We have irradiated ZrC samples at room temperature with slow heavy ions (4 MeV Au, fluence from $10^{11}$ to $5\times10^{15}$ cm$^{-2}$) in order to simulate neutron irradiations. Grazing incidence X-Ray diffraction (GIXRD) and transmission electron microscopy (TEM) analysis have been performed in order to study the microstructural evolution of the material versus ion fluence. A high sensitivity to oxidation is observed with the formation of zirconia precipitates during the ion irradiations. Three damage stages are observed. At low fluence ($<10^{12}$ cm$^{-2}$), low modifications are observed. At intermediate fluence, high micro-strains appear together with small faulted dislocation loops. At the highest fluence ($>10^{14}$ cm$^{-2}$), the micro-strains saturate and the loops coalesce to form a dense dislocation network. No other structural modification is observed. The material shows a moderate cell parameter increase, corresponding to a 0.6 vol.% swelling, which saturates around $10^{14}$ ions/cm$^2$, i.e., a few Zr dpa. As a result, in spite of a strong covalent bonding component, ZrC seems to have a behaviour under irradiation close to cubic metals.


*PACS:* 61.82.−d; 61.80.Jh; 61.10.Nz; 87.64.Bx; 61.72.Ff; 61.72.Hh; 61.72.Ji; 61.72.Nn

## 1. Introduction

In the frame of the Generation-IV international project [1], some nuclear plants are planned to work either at very high temperature or require fast neutron spectra. Those requirements lead to the selection of refractory materials with negligible neutron absorption or slowing-down cross-sections. Among the possible materials, carbides such as silicon carbide (monolithic or composites) or transition metal carbide (ZrC, TiC) are considered for some components of the reactors cores.

Zirconium carbide has been irradiated in nuclear reactors, mainly in order to study the macroscopic properties of the material (swelling, thermo-mechanical properties) or as a component of the Triso fuel particles. Most of those studies have been performed in the 1980s. They have shown a moderate damage. Particularly, the structural swelling after neutron irradiation at room temperature saturates around 1 vol.% at a few dpa's [2]. Zirconium carbide has shown a better behaviour than silicon carbide for the barrier layer of the Triso particles, higher stability at high temperature and better fission products retention [3]. Neutron irradiations of different $ZrC_x$ compounds have been performed in order to study the stability in a large stoichiometry range [4]. They show that the sub-stoichiometric materials damage relatively less than the nearly-stoichiometric ones. This is attributed to the possibility for the displaced carbon atoms to recombine with structural vacancies. Recent studies report the behaviour after ion irradiation, mainly at room temperature [4,5]. TEM examinations after irradiation with 1 MeV Kr ions [5] show the main features of the irradiated materials are surface

* Corresponding author. Tel.: +33 0 1 6908 5857; fax: +33 0 1 6908 7130.
*E-mail address:* dominique.gosset@cea.fr (D. Gosset).

0022-3115/$ - see front matter © 2007 Elsevier B.V. All rights reserved.
doi:10.1016/j.jnucmat.2007.05.034

defects due to ion milling and unidentified nanometric precipitates. No significant difference is observed after ion irradiation at 800 °C. After 2.6 MeV proton irradiation, Allen [6] has shown the formation of faulted dislocation loops at room temperature.

Zirconium carbide has a B1 (NaCl) structure, consisting in two intercalated face-centred sub-networks, respectively, Zr and C. The carbon sub-network is partially vacant, with a possible vacancy concentration ranging from a few percent (stoichiometric ZrC does not exist) to more than fifty percent. Some experimental results show that the vacancies in the sub-stoichiometric compounds can order, leading to substructures such as $Zr_2C$ [7]. A strong covalent Zr–C bonding confers its mechanical properties to the material, which is refractory (melting temperature around 3400 °C) but has a brittle mechanical behaviour (brittle–ductile transition around 1200 °C [8], low dislocation density). The density of states shows a non-vanishing electron density at the Fermi level, leading to a metal-like electron conductivity [9]. However, this low electron density at the Fermi level induces a resulting electronic thermal conductivity which is nearly equal to the phonon conductivity for the nearly-stoichiometric compounds. Moreover, the electronic thermal conductivity quickly decreases as the carbon vacancy density increases [10]. Such a complex metallo-iono-covalent bonding could have consequences regarding the nature and the behaviour of the defects produced under irradiation.

This unusual bonding leads us to study the structural evolution of zirconium carbide under irradiation. Ion irradiation have been performed with low energy heavy ions: in this case, a high density of cascades is created, leading to defect structures different of those arising from irradiations by electrons (short range displacement of isolated atoms) or protons (low density of small cascades). In order to analyse the structural evolution of the material as a function of fluence, we have then performed first Grazing-Incidence X-Ray Diffraction (GIXRD) and second, Transmission Electron Microscope observations. This allow us to identify a connection between the structural evolution and the extended defects induced by ion irradiation.

## 2. Experimental

### 2.1. Samples

The samples have been obtained by hot-pressing (1800 °C, 50 MPa, 1 h in a graphite die) of a commercial powder (Goodfellow) with grain size ~20 μm and purity > 99%. The density of the pellets is around 85%. WDS analysis on the hot-pressed material show an oxygen content < 3000 ppm.

### 2.2. Ion irradiations

The main irradiation damage in a nuclear core of inert materials such as zirconium carbide is primarily due to atomic displacements by fast neutrons. Such damages are roughly simulated by irradiations by slow heavy ions [11]. On Fig. 1 is reported the probability density function of Primary Knocked-on Atoms (PKAs) in ZrC for irradiations by 4 MeV Au ions as compared with neutrons irradiations in High Temperature Reactors (HTR, thermal neutron spectrum) and Fast-neutron Breeder Reactors (FBR, fast neutron spectrum). The maxima of the curves are very close, this means that the more probable cascades are initiated by PKAs of nearly the same energy. But it appears that in a FBR, the probability of high energy PKAs is higher, leading to a higher probability of large cascades, with heterogeneous vacancies and interstitials distributions. On the other hand, for a given fluence, the density of the cascades is lower in the case of neutron irradiations. Nevertheless, in all cases, the main part of the energy transfer is due to ballistic collisions with the atoms of the materials.

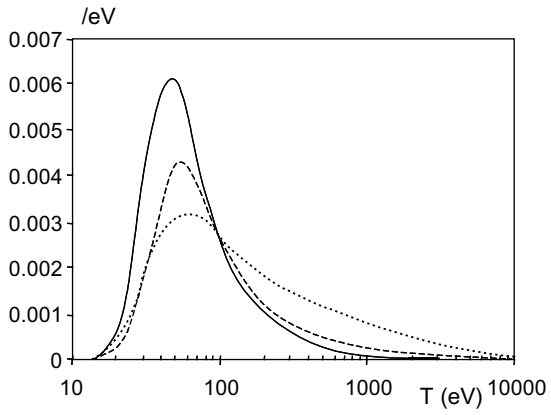


Fig. 1. Probability density of PKAs (primary knocked atoms) in ZrC irradiated in different conditions, estimated with DART [11]. Full line: 4 MeV Au ions. Broken line: HTR neutron spectrum. Dotted line: FBR neutron spectrum.

The irradiations have been performed in CSNSM Orsay (CNRS-IN2P3) on the IRMA facility with 4 MeV gold ions at room temperature. The fluence ranges from

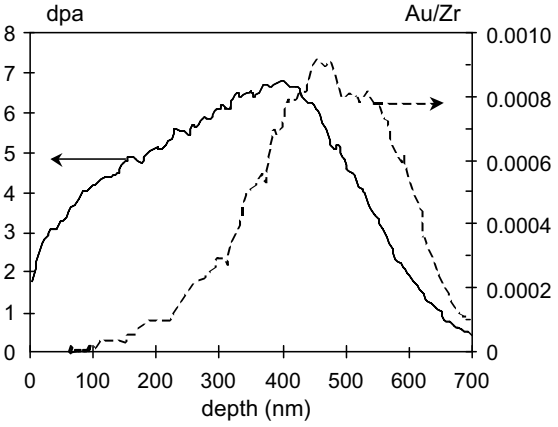


Fig. 2. SRIM estimation of damage (full line) and Au implantation (broken line) in ZrC irradiated with $1 \times 10^{15}/cm^2$ 4 MeV Au ions.

$1 \times 10^{12}$ to $5 \times 10^{15}$ ions/cm$^2$. On a first approximation, the initial damage has been estimated with the SRIM program [12] with threshold displacement energies of, respectively, 35 eV and 25 eV for Zr and C, as estimated from the values observed in TaC [13]. The damage curves are reported in Fig. 2. In the first 300 nm, the concentration of implanted ions is negligible. Consequently, the subsequent analysis (X-ray diffraction and TEM) have to be restricted to this zone, in order not to see the underlying implanted material.

## 3. Grazing incidence X-ray diffraction

In order to analyse the structural modifications of the material in the ion irradiated, damaged areas, we first used a X-ray diffraction method. The low damaged thickness then requires X-ray analysis in grazing incidence conditions (GIXRD). This is obtained with an asymmetrical configuration [14]. The diagrams are recorded with a INEL-CPS120 diffractometer (channel width = 0.015° $2\theta$). The incident beam is monochromatic (Cu K$\alpha_1$), has negligible equatorial divergence (plane (1 1 1) Ge monochromator), a 40 μm width (Gaussian-like profile) and a reduced axial divergence (~0.5°) thanks to perpendicular Sollers slits. The position of the sample with respect to the incident beam can be tuned at ±2 μm and ±0.02°. The analysis have been performed with an incident beam at 0.70° incidence angle, leading to an analysed depth around 300 nm (Fig. 3).

### 3.1. Microstructure evolution

The modifications of the microstructure of the material is obtained by an analysis of the evolution of the profile of the diffraction lines. These profiles result from the convolution of instrumental and material components. Due to large instrumental breadths, only the evolution of the integral breadths of the lines can be analysed. Here we have represented the angular variation of the material component by the Hall–Williamson approximation, leading to the classical separation of size and distortion (microstrains) effects

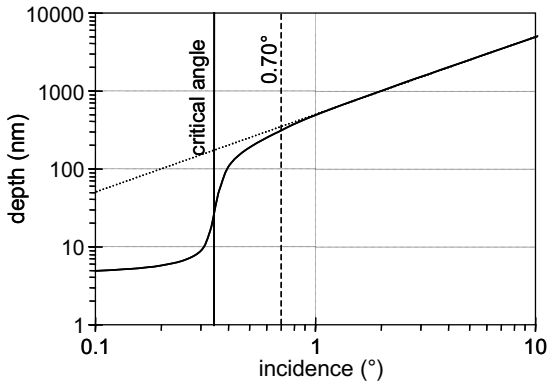


Fig. 3. Material thickness contributing to 90% of the detected X-rays versus the angle of the incident beam for ZrC. Classical approximation (no refraction): dotted line. With refraction: full line.

$$\Delta\beta_m = \frac{\lambda}{d\cos(\theta)} + 4\varepsilon\tan(\theta), \tag{1}$$

where $\Delta\beta_m$ is the variation of the material component to the integral breadth $\beta$ of the lines, defined as $\beta = \int I(2\theta)d2\theta / I(2\theta_0)$, before and after irradiation, $d$ is the size of the coherent diffracting domains, and $\varepsilon$ is the strain dispersion in the domains.

Here, due to the grazing incidence condition which induces a very broad X-illuminated area, a large instrumental component superposes to the material ones. This instrumental line-width varies as

$$\beta_I = \frac{w}{R}\frac{\sin(2\theta - \varphi)}{\sin\varphi}, \tag{2}$$

where $w$ is the width of the incident beam (nearly purely Gaussian profile with FWHM around 40 μm), $R$ the radius of the goniometer (250 mm) and $\varphi$ the incidence angle (0.70°). This contribution (around 0.75° at $2\theta = 90°$) has then an angular variation clearly different of the material components (size and strain) and can be easily removed.

The microstructure parameters are deduced from the diagrams according to two complementary analysis methods.

- First, the line breadths are obtained with a line to line analysis. The profiles are here fitted by pseudo-Voigt functions. A least squares calculation on the resulting integral breadths have been performed according to Eqs. (1) and (2).
- Second, the unit-cell parameter is deduced from a Rietveld analysis in the full pattern matching (FPM) mode with the XND program [15]. As compared with a structural refinement, the correlations between the intensities of the lines are here removed. This allows a better description of the line profiles. This results in a better sensitivity on their positions which leads to more accurate estimations of the unit cell parameter.

### 3.2. Structure refinement

Structural Rietveld refinements have been performed in order to analyse possible evolutions of the structure of ZrC such as space group modifications (substructures) or disorder. The initial structure is the rock-salt structure of the non-irradiated ZrC ($Fm\bar{3}m$).

## 4. Transmission electron microscopy

The observations have been performed on a JEOL-1200 EX TEM. Discs with diameter 3 mm and thickness 150 μm have been prepared by classical machining and polishing. Thanks to the metallic character of zirconium carbide, electrochemical polishing has been used to obtain the samples (Tenupol III® with 721 solution: 70 vol.% ethanol, 20 vol.% glycol–ethylene monobutylic-ether, 10 vol.%

perchloric acid). Owing to the fragility of the discs, some of them have been polished in two steps, one face prior the irradiations and the second one after.

## 5. Results

### 5.1. X-ray diffraction

The evolution of the diffraction diagrams as a function of fluence is reported on Fig. 4. The intensity of the baseline is very low, no amorphisation can be observed. Slight variations of the background and the scale factor are observed, which may be attributed to a low disorder. A strong broadening of the ZrC lines can be seen as the fluence increases. Due to the very high sensitivity to sample decentring of the GIXRD method, the apparent position of the lines is here meaningless for an estimation of a possible cell parameter variation.

The cell parameter evolution is obtained from a Rietveld analysis in the FPM mode. We observe the cell parameter increases up to $1 \times 10^{14}/cm^2$ then remains nearly constant (Fig. 5). The corresponding volume swelling is around 0.6 vol.%. The instrumental broadening parameter leads to an apparent beam width in the range 35–45 μm, close to the actual width of the slits.

In Fig. 6 we present a Hall–Williamson plot of the integral breadths for different fluences. The individual integral breadths are deduced from the line-to-line analysis after

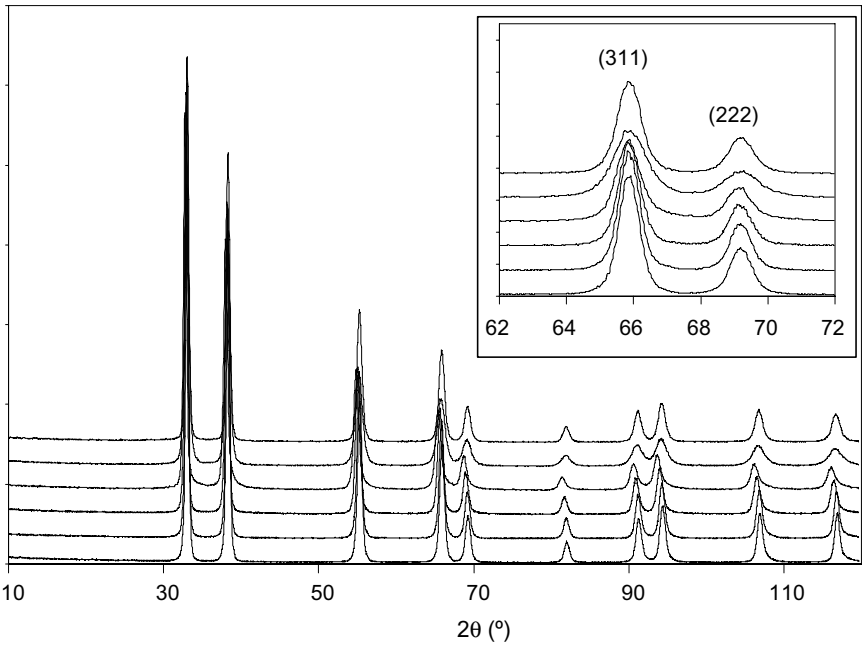


Fig. 4. Diffraction diagrams in grazing incidence conditions (incidence angle = 0.7°) of micrometric ZrC implanted with Au (4 MeV) ions. Fluences, from bottom to top: 0, $1 \times 10^{12}$, $1 \times 10^{13}$, $1 \times 10^{14}$, $1 \times 10^{15}$, $5 \times 10^{15}/cm^2$ (diagrams shifted for clarity). The insert evidences the broadening of the lines at the highest fluences.

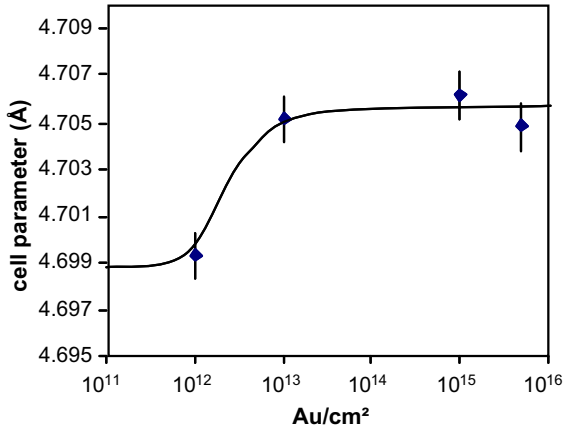


Fig. 5. Evolution of the cell parameter of ZrC as a function of Au (4 MeV) fluence.

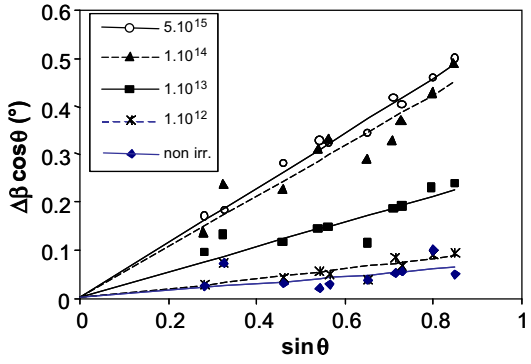


Fig. 6. Hall–Williamson plots of the integral breadths of the lines versus Au fluence (instrumental broadenings removed). Points: from line-to-line analysis. Solid lines: least squared calculations.

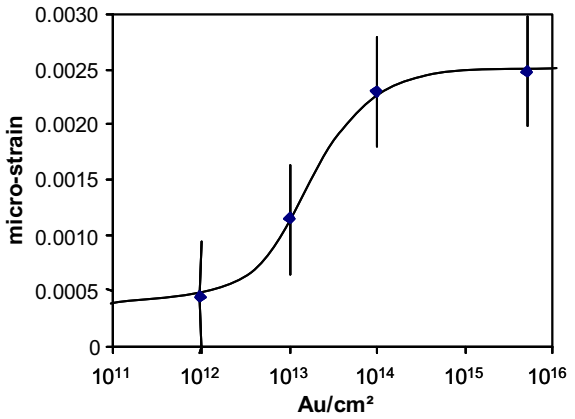


Fig. 7. Evolution of the micro-strains as a function of Au fluence as deduced from the slope of the Hall–Williamson plots.

removal of the $\sin(2\theta - \varphi)$ instrumental component. The plots show there is no significant evolution of the size of the diffracting domains ($\Delta\beta$ close to 0 at $\theta = 0$). The broadening is then purely associated to micro-strains (slope of the plots). The micro-strains are negligible up to a fluence of around $10^{12}$ Au cm$^{-2}$, then they increase sharply up to around $10^{14}$ Au cm$^{-2}$ and remain constant at the highest fluences (Fig. 7).

Structural Rietveld refinements of the crystal structure as a function of fluence lead to good reliability factors (RB $< 2\%$). As a consequence, there is no significant change of the crystal structure of the material and the initial $Fm\bar{3}m$ structure is not modified during irradiation. However, the large breadths of the lines due to the grazing incidence setup prevent the observation of weak lines. The formation of small precipitates or substructures, leading to the formation of extra but very weak lines [7], could then not be observed.

### 5.2. Transmission electron microscopy

The TEM observations have been performed on materials irradiated at three different fluences, $1 \times 10^{13}$, $5 \times 10^{14}$ and $5 \times 10^{15}$ Au/cm$^2$. Due to the porosity of the materials, the TEM samples show limited observation areas. On the other hand, the degradation of the samples surface during irradiation (cf. infra) lead to bad quality photographs which prevent a deep analysis of the irradiation defects.

As a function of fluence, a significant evolution can be observed (Fig. 8). At the lowest fluence, the material shows nearly no contrast (very low dislocation density). At $5 \times 10^{14}$/cm$^2$, a high density of small defects with strong contrasts is observed. Observations in the diffraction mode shows weak streaks connecting the (1 1 1) to the (2 2 0) reflections (Fig. 9). At the highest fluence, the small defects are replaced by a dense dislocation network.

On the other hand, we observe the formation of a second phase after the irradiations. This phase appears first as incomplete rings of dots on the diffraction photographs (Figs. 9 and 10) with an intensity and a homogeneity increasing with fluence. On the most irradiated sample, several rings are clearly visible. From their relative radii and intensities, it appears that these rings no longer correspond to the initial ZrC cubic phase and should be attributed to a quadratic phase. The cell parameters we then deduce from

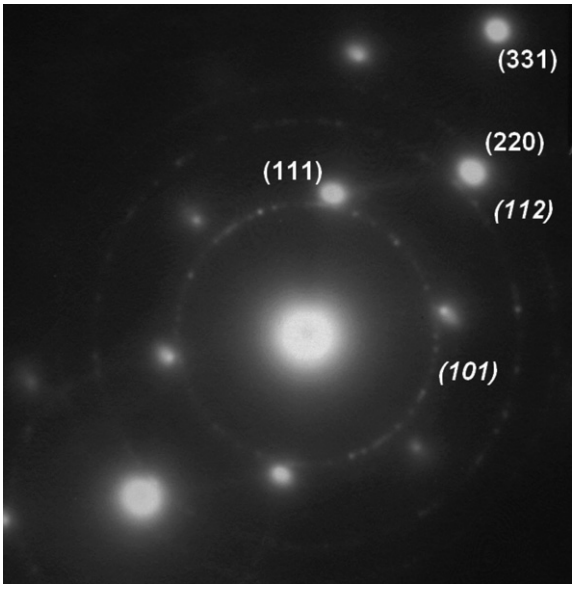


Fig. 9. TEM examination in diffraction mode of the $5 \times 10^{14}$/cm$^2$ irradiated ZrC sample. ($hkl$): ZrC spots. Italic ($hkl$): rings corresponding to nanometric quadratic $ZrO_2$ grains. Weak streaks connect the (1 1 1) to the (2 2 0) reflections.

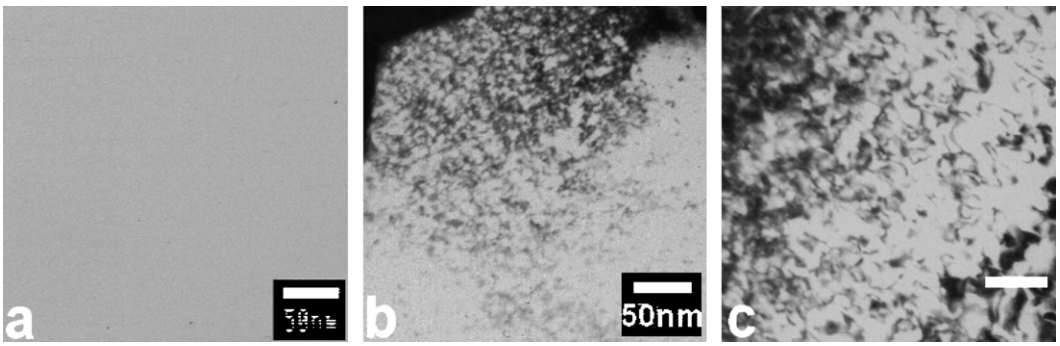


Fig. 8. TEM observations ((2 2 0) dark field) of Au 4 MeV irradiated ZrC. (a) $1 \times 10^{13}$/cm$^2$. (b) $5 \times 10^{14}$/cm$^2$. (c) $5 \times 10^{15}$/cm$^2$. bar: 50 nm.

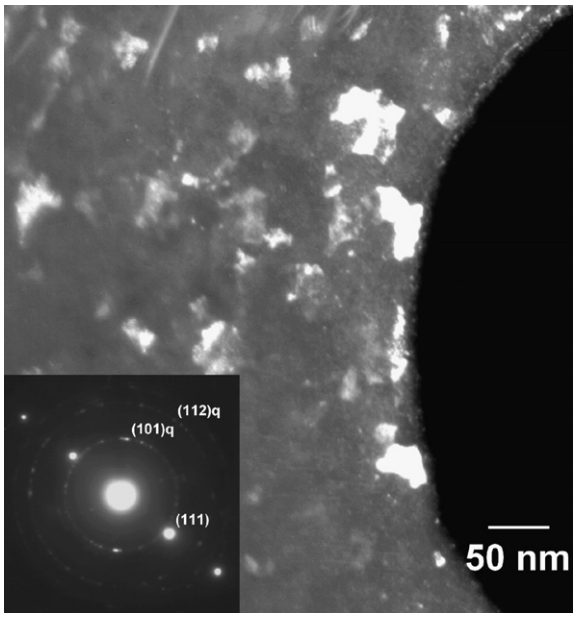


Fig. 10. TEM examination of the $5 \times 10^{15}/cm^2$ irradiated ZrC sample. Dark field with a part of the quadratic $ZrO_2$ (101)q ring.

the TEM diffraction patterns are similar to those of quadratic zirconia ($a \approx 3.61$ Å, $c \approx 5.19$ Å). Dark field observations with a part of the most intense ring (Fig. 10) show a high density of nanometric precipitates. Tilting of the sample clearly shows that they are located on the surfaces of the sample, either the front surface for the samples thinned in two steps, before and after irradiation, or the two surfaces for the samples totally thinned prior to the irradiation. Moiré fringes show that the precipitates have grown partially coherently with the bulk material.

## 6. Discussion

The observations we have performed here show that zirconium carbide presents a low damage under ion irradiation at room temperature. The cell parameter variation is low and shows a saturation for a few displacements per atoms. Those results are in agreement with previous observations performed in zirconium carbide irradiated at room temperature in a nuclear reactor [2]. Such a low swelling can be partly attributed to the high vacancy density on the carbon sub-network which allows a high mobility of the carbon defects, this preventing their aggregation. This effect has previously been observed in a sub-stoichiometric tantalum carbide [13].

The irradiation defects produced at the lowest fluences ($<10^{12}$ Au cm$^{-2}$) have not been identified here but they induce no significant modification of the material (swelling and micro-strains). At intermediate fluence ($<10^{14}$ Au cm$^{-2}$), a high density of defects associated with high internal stresses are produced. The streaks which appears between the TEM diffraction spots (Fig. 9) can be attributed to stacking faults. On the other hand, molecular dynamic simulations have shown the formation of small faulted dislocation loops in the core of a cascade [16]. Such observations agree with previous analysis performed by Allen [6] in zirconium carbide irradiated with protons. As a consequence, we may assume that the defects here produced are small faulted loops. Moreover, we deduce from our results and Allen observations that the nature of these defects does not depend on the initial damage, large and dense displacement cascades in the case of the Au ions or small and spread ones in the case of the protons. At fluences above $10^{15}$ Au cm$^{-2}$, these loops grow and coalesce, this leading to the formation of a dense dislocation network. This network could then achieve an efficient trapping of the defects and then a saturation of the internal strains and of the swelling as observed by X-ray diffraction.

On the other hand, we observe a second phase after the ion irradiation. This phase can be identified as precipitates of quadratic zirconia. Such an evolution of the material has been previously reported by Gan [5], the second phase he observed can then also be identified to quadratic zirconia. The precipitates are located on the surfaces of the samples. The quadratic phase of zirconia is here stabilized thanks to the nanometric size of the grains [17]. A consequence of this precipitation is that only poor quality TEM observations can be performed at high fluence and accurate identification of the irradiation defects can no longer be done. However, the main result is that these oxide precipitates are observed after the irradiations in the vacuum chamber of the accelerator and then emphasises the high sensitivity of zirconium carbide to oxidation. This should have to be taken into account for the possible use of this material in the future planned nuclear reactors. As a matter, it appears that it should not be used without protective layers or shields preventing any direct contact with an oxidizing media such as oxide fuel or cooling fluid.

## 7. Conclusion

We have performed Au 4 MeV ion irradiations of zirconium carbide at room temperature. Rietveld analysis of the X-ray diffraction patterns show a moderated swelling and high internal stresses which both saturates at a Au fluence around $10^{14}$ cm$^{-2}$ corresponding to a few dpa's. TEM observations show the formation of a high density of small faulted dislocation loops which lead to the formation of a dense dislocations network at the highest fluences. As a consequence, this material behaves under ion irradiation nearly like a cubic metal. The complex bonding appear to have low consequences regarding the evolution of the defects. On the other hand, the material appears very sensitive to oxidation, with the observation of zirconia precipitates at the samples surfaces after the irradiations. Further studies should be performed, to improve the identification of the defects and their dynamics (growth, coalescence, annealing) as a function of flux, fluence, temperature and stoichiometry.

## Acknowledgements

We are very indebted to Thierry Vandenberghe (CEA Saclay, DMN/SRMA) for the TEM observations. Laurent van Bruetzel (CEA-Valrho, DRPC) has performed very useful molecular dynamic simulations. This work was supported by the CEA-CNRS Research Group ISMIR.

## References

[1] <http://www.gen-4.org/>.
[2] M.S. Koval'chenko, Yu.I. Rogovoi, Inorg. Mater. 9-2 (1973) 290.
[3] K. Minato, T. Ogawa, K. Sawa, A. Ishikawa, T. Tomita, S. Iida, H. Sekino, Nucl. Technol. 130 (2000) 272.
[4] R.A. Andrievskii, V.I. Savin, V. Ya Markin, V.T. Spravtsev, A.S. Shevshenko, Inorg. Mater. 14-4 (1978) 526.
[5] J. Gan, Gas-Cooled Fast Reactor (GFR), FY04 Annual Report, INEEL/EXT-04-02361, 2004.
[6] T. Allen, NERI Quaterly Progress Report, 2006.
[7] A.I. Gusev, A.A. Rempel, A.J. Magerl (Eds.), Disorder and Order in Strongly Non-stoichiometric Compounds, Springer, 2001.
[8] R. Darolia, T.F. Archbold, J. Mater. Sci. 11 (1976) 283.
[9] H. Ihara, M. Hirabayashi, H. Nakagawa, Phys. Rev. B 14-4 (1976) 1707.
[10] E.K. Storms, P. Wagner, High Temp. Sci. 5 (1973) 454.
[11] L. Lunéville, D. Simeone, C. Jouanne, J. Nucl. Mater. 353 (1–2) (2006) 89.
[12] J. Ziegler, <http://www.srim.org>.
[13] D. Gosset, thèse Orsay, 1985.
[14] D. Siméone, D. Gosset, J.L. Bechade, A. Chevarier, J. Nucl. Mater. 300 (2002) 27.
[15] J.F. Bérar, G. Baldinozzi, CPD Newslett. 20 (1998).
[16] L. van Bruetzel, J.P. Crocombette, Nucl. Instrum. and Meth. B 255 (2007) 141.
[17] G. Baldinozzi, D. Simeone, D. Gosset, M. Dutheil, Phys. Rev. Lett. 90 (2003) 216103.